UC Santa Barbara

UC Santa Barbara Previously Published Works

Title

Tuning nuclear depolarization under MAS by electron T 1e

Permalink

https://escholarship.org/uc/item/7mz1487j

Journal

Physical Chemistry Chemical Physics, 20(37)

ISSN

0956-5000

Authors

Lund, Alicia
Equbal, Asif
Han, Songi

Publication Date

2018-10-07

DOI

10.1039/c8cp04167a

Peer reviewed

eScholarship.org Powered by the California Digital Library
University of California

Author Manuscript

Author Manuscript

Author Manuscript

Author Manuscript

HHS Public Access

Author manuscript

Phys Chem Chem Phys. Author manuscript; available in PMC 2019 October 07.

Published in final edited form as:

Phys Chem Chem Phys. 2018 October 07; 20(37): 23976–23987. doi:10.1039/c8cp04167a.

Tuning nuclear depolarization under MAS by electron T_{1e}

Alicia Lund[a], **Asif Equbal**[a], and **Songi Han**[a,b,*]

[a]Department of Chemistry and Biochemistry, University of California Santa Barbara, Santa Barbara, CA 93106-9510, USA.

[b]Department of Chemical Engineering, University of California Santa Barbara, Santa Barbara, CA 93106-9510, USA.

Abstract

The Cross-Effect (CE) Dynamic Nuclear Polarization (DNP) mechanism under Magic Angle Spinning (MAS) induces depletion or "*depolarization*" of the NMR signal, in the absence of microwave irradiation. In this study, the role of T_{1e} on nuclear depolarization under MAS was tested experimentally by systematically varying the local and global electron spin concentration using mono-, bi- and tri-radicals. These spin systems show different depolarization effects that systematically tracked with their different T_{1e} rates, consistent with theoretical predictions. In order to test whether the effect of T_{1e} is directly or indirectly convoluted with other spin parameters, the tri-radical system was doped with different concentrations of $GdCl_3$, only tuning the T_{1e} rates, while keeping other parameters unchanged. Gratifyingly, the changes in the depolarization factor tracked the changes in the T_{1e} rates. The experimental results are corroborated by quantum mechanics based numerical simulations which recapitulated the critical role of T_{1e}. Simulations showed that the relative orientation of the two *g*-tensors and *e-e* dipolar interaction tensors of the CE fulfilling spin pair also plays a major role in determining the extent of depolarization, besides the enhancement. This is expected as orientations influence the efficiency of the various level anti-crossings or the "*rotor events*" under MAS. However, experimental evaluation of the empirical spectral diffusion parameter at static condition showed that the local vs. global *e-e* dipolar interaction network is not a significant variable in the commonly used nitroxide radical system studied here, leaving T_{1e} rates as the major modulator of depolarization.

Graphical Abstract

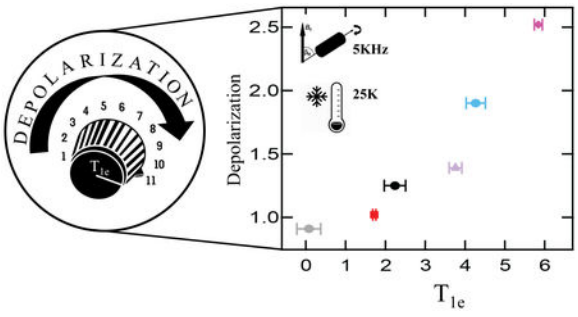

*corresponding author: songi@chem.ucsb.edu.

Author Manuscript Author Manuscript Author Manuscript Author Manuscript

T_{1e} modulates nuclear depolarizarion in Cross-Effect Dynamic Nuclear Polarizarion under Magic-Angle Spinning

1. Introduction

Dynamic Nuclear Polarization (DNP) combined with Magic Angle Spinning (MAS) Nuclear Magnetic Resonance (NMR) has been shown to be a powerful tool for elucidating molecular structure information of a variety of biological compounds[1–3] and material surfaces.[4–7] The signal enhancement from MAS-DNP has led to drastic time savings, easily reducing experimental time from days to hours and enabling NMR experiments that were not feasible before, such as heteronuclear correlation measurements with low natural abundance nuclei.[8,9] DNP is a method of transferring the magnetization or polarization from unpaired electron spins from a polarizing agent, typically a free radical, to nuclear spins that are dipolar coupled to the unpaired electron spins of the radical. Because of the potential of DNP to fundamentally transform the capabilities of solid-state MAS NMR, much work has gone into rationally designing radical-based DNP agents to obtain maximum signal enhancements or other favorable properties at high magnetic fields and faster spinning frequency.[10–17]

The key performance metrics for DNP include a high NMR signal enhancement factor, a short DNP build-up time constant, and a minimal reduction of the thermally polarized NMR signal by the paramagnetic bleaching effect, and the more recently discovered depolarization mechanism operational under MAS. Depolarization under MAS occurs independent of microwave (μw) irradiation, as will be discussed in the theory section. The focus of this study is to understand the role of electron spin dynamics in tuning depolarization, which is quantified as the ratio of NMR signal under spinning and static condition, in the absence of μw irradiation, i.e., $\epsilon_{depo} = \langle S_{spin} \rangle / \langle S_{static} \rangle$. Much of the current development has focused on synthesizing and testing tethered nitroxide bi-radicals such as TOTAPOL,[10] AMUPOL[18] and TEKPOL,[15] while there are also studies of tri-radicals such as DOTOPA[19] and mixed multi-radicals.[20,21] However, the design principle for multi-radicals that yield the strongest DNP performance, in particular under MAS conditions, is still debated and relies on empirical testing, as the performance-driving factors are not entirely understood. The complexity comes from the strong dependence of the DNP performance on many interconnected internal parameters, such as temperature, relaxation rates, radical concentration, glass forming quality of the solvent, and external parameters such as the main magnetic field, the MAS frequency and the μw field strength. Apart from this, the relative orientation of the *g*-tensors, and the electron-electron (*e*-*e*) coupling tensors are also dominant factors modulating the DNP performance. Despite the recognition that there are a multitude of interrelated factors, a general presumption is that designing DNP polarizing agents with long electron spin lattice relaxation times, T_{1e}, is a desirable design principle for achieving high DNP performance through better electron spin saturation.[15] However, long T_{1e} also enhances the depolarization mechanism, adversely affecting the DNP performance. The question we ask is whether the effect of T_{1e} a dominant factor in tuning the depolarization effect among different DNP polarizing agents under available experimental conditions for DNP. We address this question with experimental and theoretical data.

Author Manuscript Author Manuscript Author Manuscript Author Manuscript

On the experimental side, we performed MAS DNP experiments at ~7 Tesla and 25 K to measure the DNP enhancement and depolarization factors, as well as the electron T_{1e} relaxation rate. We compared these properties between a mono-, di- and tri-nitroxide radical, while also deliberately shortening the T_{1e} through the addition of a paramagnetic relaxation agent, $GdCl_3$, without affecting other relevant factors of the spin system (*e-e* and *e-n* interaction tensors) for DNP. We also measured the electron spin saturation and spectral diffusion parameters (under static conditions) of various mono-, bi-, and tri- nitroxide radicals to evaluate the strength and property of the *e-e* dipolar interaction network. Finally, we correlated experimental T_{1e} data with the extent of nuclear spin depolarization under MAS.

The experimental observations are corroborated with quantum mechanical numerical simulations of a coupled *e-e-*^{1}*H* three spin system using the SpinEvolution package[22] that recently introduced the pseudo secular *e-n* hyperfine interactions to enable DNP simulations under MAS. Through simulations, we estimated the influence of T_{1e} on nuclear depolarization. There is a significant body of theoretical work on calculating DNP enhancements and depolarization effects under MAS that inspired this study.[23–27] However, this is the first report to calculate MAS DNP parameters using SpinEvolution which is an exceptionally effective program, yielding the calculation of 3-spins with 100 orientations within two minutes. Comparison and validation on select calculations using SpinEvolution are provided in the supplementary information (SI). Also, the calculation is based on fully quantum mechanical descriptions, without the Landau-Zener (LZ) assumption for the *e-e-*^{1}*H* transitions.

2. Cross effect theory under MAS

Presumably, the most effective DNP mechanism under MAS is the cross effect (CE).[28] This will be the mechanism of concern in this paper for delineating the effect of electron spin dynamics on nuclear depolarization under MAS-DNP conditions. To do so, we first briefly discuss the basic theory behind CE. Pedagogically, the CE mechanism can be defined as the following: two dipolar or exchange coupled electron spins with a frequency difference that is approximately equal to a hyperfine coupled nuclear Larmor frequency undergo an energy conserving flip-flop process that can cause the simultaneous flips of the two electron spins and the nuclear spin, *i.e.* when ω_{e1}-ω_{e2}=ω_n, where ω_{e1}, ω_{e2} and ω_n are the Larmor frequencies of the two electrons and the nucleus, respectively. Such flip-flop in the spin states leads to transfer of polarization amongst the spins. The amount of polarization transfer to the nuclear spin from the electron spin is proportional to the difference in the two electron spin polarizations relative to the nuclear spin polarization. Therefore, driving the spin system towards a larger electron spin polarization difference is essential for achieving significant DNP transfer. Ideally, selective μw irradiation on one of the two coupled electron spins should be used to create a large polarization difference between the two electron spins that fulfill the CE condition. Practically, this is achieved through the saturation of a portion of the EPR spectrum of the nitroxide radical- the polarization difference between electrons is subsequently transferred to the coupled nuclear spins.

Author Manuscript Author Manuscript Author Manuscript Author Manuscript

All of the above holds true for static samples, but the CE under MAS becomes considerably more complex. Nuances about the CE mechanism under MAS have been contributed by the groups of Tycko and Vega.[23-25] In static samples, the energies of the spins are fixed in time, and therefore the same pairs of electron spins always fulfil the CE condition, while under MAS the matching conditions change in time. This is because the large *g*-anisotropy of the nitroxide radical causes the resonance frequency of the electron spin to oscillate over the course of the MAS rotor period, causing multiple different energy level-crossings and anti-crossings of dipolar coupled electron spins throughout the rotor period, as first detailed by Thurber *et. al.*[25] Some of these resonances fulfill the CE conditions with respect to the nuclei, leading to polarization exchange between the electron spins and the nuclei. These energy oscillations owing to MAS increase the combinations of spin pairs fulfilling the CE conditions. Important to note - while the number of crossings per unit time is directly proportional to the spin rate and depends on the orientations of the spin interaction tensors, the effectiveness of the anti- or avoided-crossing depends on the magnitude of the *e-e* and the *e-n* couplings (*i.e.* the strength of the perturbations, or the off-diagonal terms) and crossing rate (*i.e.* the rate of change in energy or the rate of change of the diagonal terms), as illustrated in the LZ expression,[25,29] which gives the probability of an adiabatic transition for two state systems. As shown in the equation below, the adiabatic transition probability is inversely proportional to the rate of change of energies of a two-state system (A), and directly proportional to the strength of perturbation (E) that mixes the two states.

$$\text{Probability (adiabatic or anti-crossing)} = 1 - \exp(-\pi E^2 / A). \quad (1)$$

Thurber and Tycko[26] were the first to uncover that the same rotor-synchronous level-crossings under MAS that lead to the enhancement, can also lead to a reduction in nuclear polarization. Without μw irradiation, *e-e* coupling at resonance conditions ($\omega_{e1} = \omega_{e2}$) causes an exchange or equalization of the polarization across the EPR line. The operational CE Hamiltonian, however, can lead to the transfer of magnetization from the nucleus to the electron spins, and therefore leading to a reduction in the nuclear spin signal.

Traditionally, DNP signal enhancements were calculated by the NMR signal area with μw irradiation divided by the NMR signal without μw irradiation, *i.e.* $\epsilon_{on/off} = \langle S_{mw\_on} \rangle / \langle S_{mw\_off} \rangle$. However, as the nuclear depolarization effect (ϵ_{depo}) artificially lowers the unenhanced (μw off) Boltzmann NMR signal, *i.e.* the denominator in calculating the enhancement factor, this effect can lead to an inflation in the DNP enhancement factor that does not represent the absolute NMR signal gain by DNP, as discussed in several recent studies.[26,27,30] The intensity of the NMR signal with μw irradiation turned off is further attenuated by paramagnetic effects (PE), but typically to a lesser extent than by depolarization by CE under MAS, especially at ultra low temperature.

There are multiple controllable factors affecting the extent of depolarization, such as the MAS frequency, the external magnetic field strength, the spin relaxation rates- electron T_{1e} and nuclear T_{1n}, and the radical concentration, apart from other intrinsic spin parameters of the radical. The dependence of spinning frequency on depolarization has been reported on in

Author Manuscript Author Manuscript Author Manuscript Author Manuscript

the literature.[26-27] Typically, faster spinning leads to greater depolarization up to a threshold spin rate when depolarization reaches a plateau value, typically between 2-5 kHz with commonly used nitroxide biradical.

The makeup of the electron spin network is another critical factor in modulating depolarization. The *e-e* coupling facilitates spin diffusion towards equalization of the polarization. Full quantum mechanical description of electron spectral diffusion is beyond the scope of present theoretical framework. However, using the LZ model the effect of inter- and intra-molecular electron coupling has been studied in biradicals, showing that intermolecular *e-e* couplings can further diminish the nuclear Boltzmann polarization compared to the case when inter-*e-e* couplings are ignored.[26,27,31]

Last, but not least, relaxation rates are critical modulators of depolarization, especially the T_1 relaxation rates as they govern the rate with which the system attains its equilibrium state when perturbed by spinning and μw. The nuclear spin relaxation rate constant, T_{1n}, directly affects the nuclear depolarization. Longer T_{1n} leads to larger depolarization and also larger enhancement. Here, it is important to point out that the T_{1n} of nuclei is shortened by faster MAS, presumably due to CE interactions as shown by Thurber *et. al.*[26] and also reported by Mentink-Vigier *et. al.*[27] The effect of the spin-lattice relaxation time of the electron spin, T_{1e}, on depolarization has also been discussed in the literature - the focus of this study. The polarization distribution across the EPR line, and therefore the polarization difference between the electron spins that fulfil the CE requirement is modified by MAS depending on the magnitude of the spin rate relative to $1/T_{1e}$, as numerically simulated at 9.4 T by Thurber and Tycko.[26] As predicted by their theoretical model, for shorter T_{1e}, the polarization difference depends linearly on the effective EPR resonance frequency following the Boltzmann distribution, but longer T_{1e} causes significant deviation from the thermal polarization condition. While MAS causes the polarization difference in electrons to generally decrease, spin-lattice relaxation restores their polarization towards the Boltzmann equilibrium if $1/T_{1e}$ is high relative to the spin rate. This finding is consequential for the tuning of DNP conditions. Many contemporary bi-radicals are designed to increase the efficacy of the CE mechanism through an increase in T_{1e} to enhance its saturability by μw irradiation, while simulations have shown that increasing the T_{1e} can also increase depolarization.[15,18] Thus presumably, there is an intermediate “Goldilock” T_{1e} value that balances these two competing effects. However, direct measurements of T_{1e} in conjunction with nuclear depolarization under MAS are not reported in the literature, and as such it is unclear whether T_{1e} is a dominant modulator of nuclear depolarization, amongst the cornucopia of factors that also modulate nuclear depolarization. Our study is narrowly focused on answering whether long T_{1e} dominantly modulates nuclear depolarization, and as such overrides other factors that modulate nuclear depolarization. We accompany our experimental observations with a fully quantum mechanical simulation of the MAS DNP effect.

Author Manuscript Author Manuscript Author Manuscript Author Manuscript

3. Methods

3.1 DNP NMR under MAS at 25 K and 7 T

NMR/DNP measurements were performed with a Revolution NMR LLC MAS probe operational at 25 K, and outfitted with a Thomas Keating Ltd. corrugated waveguide inside a 7 T Bruker wide bore magnet. The design of the low temperature (LT) MAS probe is a replication of the Thurber and Tycko design as published recently and relies on nitrogen and helium gas for spinning and cooling the sample, respectively.[32,33]

A Virginia Diode Inc. μw source with a frequency range from 193-201 GHz with nominal output power of 140 mW was employed in a quasi-optical (QO) DNP bridge as shown in Fig. 1. Two parabolic focusing mirrors focus/converge the μw beam into the corrugated waveguide that extends from the top of a MAS probe. Room temperature nitrogen gas is used for the bearing and drive of the probe, and cold helium gas is used to cool the sample space, using a stator similar to that described by Thurber *et. al.*[32,33] A solution of each radical species was made by dissolving the radicals in 60:30:10 v/v% D_8-glycerol:D_2O:H_2O at a 20 mM global electron spin concentration.

A zirconia rotor with an outer diameter of 4 mm, an inner diameter of 2.36 mm, a length of 46 mm, and a total sample volume of 0.044 ml was employed. The sample was centred in the rotor using two teflon spacers at its either ends. The sample was packed by first loosely packing 60 mg of KBr, then pipetting 20 mg of the radical solution into the rotor and gentle mixing. Here, KBr was added in order to monitor the sample temperature *in situ* through the measurement of ^{79}Br T_{1n} as shown by Thurber *et. al.*[34] The resulting NMR signal was recorded with a Bruker 300 MHz spectrometer. The packed rotor was placed in the MAS stator and liquid helium was used to cool the sample space until an average LT of 25 K was reached (1 litre⁄hour), while room temperature nitrogen gas (10 litre⁄hour) was used for the bearing and drive pressure. For sanity check, the sample temperature was recorded by measuring the T_{1n} of ^{79}Br before and after the enhancement measurement, and confirmed that an average sample temperature at 25 K ± 2 K was maintained.

3.2 Pulsed EPR under static conditions at 25 K and 7 T

All EPR measurements were performed using the Han lab's home-built dual static DNP/EPR spectrometer operating at 193-201 GHz, as described above and published elsewhere.[35,36] This spectrometer employs the same Virginia Diode Inc. μw source as used in the MAS-DNP measurements. A QO scheme focuses the Gaussian μw beam to a corrugated waveguide positioned in the center of a home built static EPR probe inside a Bruker 7 T wide bore magnet, as described in an earlier publication.[35] This EPR spectrometer employs a phase sensitive induction mode detection scheme, where the ~200 GHz EPR signal is mixed down to 3 GHz, then mixed with a 3 GHz reference signal. The DC in-phase and out-of-phase signal components are then processed using the SpecMan4EPR software. Details of the dual EPR/DNP spectrometer quasi-optic, probe, and detection design are detailed by Siaw *et. al.*[35] The electron spin-lattice relaxation time (T_{1e}) of the nitroxide radical solutions were measured using a saturation recovery solid echo detection pulse sequence. For ELDOR measurement, the pump frequency is stepped across

Author Manuscript Author Manuscript Author Manuscript Author Manuscript

the entire EPR spectrum while the probe frequency is held constant. Two VDI solid-state microwave sources were employed for ELDOR experiments--one for pump (saturation) frequency and the other for probe (detection) frequency.[37] Two sources are necessary because the process of changing between two microwave frequencies is longer than the delay used between the excitation and detection pulses for ELDOR measurements. Additionally, the use of two sources allows for background free ELDOR acquisitions due to hysteresis that can occur between the pump and probe frequencies. We note that both T_{1e} and ELDOR experiments were performed under static conditions, but at otherwise comparable temperature and magnetic field.

3.3 Numerical Simulations

The numerical simulation shown in this manuscript were performed using the SpinEvolution package, which is a widely used software for NMR simulation, especially for solid state powder sample.[22] Recently, the package's capability has been extended to perform DNP simulation through the incorporation of the *e-n* pseudo secular hyperfine coupling term in the internal Hamiltonian, providing a platform for fast and efficient DNP simulations.[22,38] This program relies on numerically solving the time-dependent von Neumann equation of motion by dividing the calculation of time evolution into multiple time-independent steps of small time intervals. This is the same approach as used in other simulation packages (*e.g.* SPINACH[39] and SIMPSON[40]), as well as the simulation programs used for MAS DNP written by Thurber *et. al.*[25] and Mentink-Vigier *et. al.*[24] However, Thurber and Mentink-Vigier incorporated the spin relaxation effect differently. In the Thurber approach, the propagator is calculated at each time step in the Hilbert space, and then the relaxation effect applied on the evolved density matrix at each step. Mentink-Vigier's calculation is performed in the Liouville space, while incorporating relaxation effects together with all other spin interactions during time-evolution. The rotor-synchronized time evolution propagator is calculated, which is then used for stroboscopic rotor-synchronized time-evolution. The SpinEvolution package offers the flexibility to use either of the two approaches by selecting the appropriate "*-lv*" option.[22] In this paper, we have used the approach used by Mentink-Vigier as it leads to faster calculation for small spin systems given the rotor-synchronization detection. However, for a larger spin system, calculations in the Liouville space calculation will get exponentially slower due the the large matrix dimensions. In such cases, calculation in the reduced Liouville space[31] or Hilbert space (Thurber's approach) would become more economical.

The simulation shown here are performed on a 3-spin system, including 2 electron spins and 1 nuclear spin. The inter-spin dipolar coupling between the electrons, e_1-e_2, electrons and nucleus, e_1-n and e_2-n, are taken to be 19 MHz (~14 Å), 2.5 MHz (~3.2 Å) and 0.08 MHz (~10 Å), respectively. The principal axis components of the *g*-tensors of the electrons are taken to be: g_x=2.0094, g_y=2.006, g_z=2.0017, inspired by nitroxide radicals. Unless otherwise mentioned, the *g*-tensor of the second electron spin is related to the first electron spin by a set of Euler angles, (70°,82°,0°) and the relative e_1-e_2 dipolar tensor orientation given by the angles (124°,94°,0°). These are pseudo-random orientations for TOTAPOL molecule. The exact orientations of these tensors are unknow due to flexibility of these molecule. The principal axis orientation of the dominant e_1-n coupling is chosen to be the

Author Manuscript Author Manuscript Author Manuscript Author Manuscript

same as the *g*-tensor of e_1. The relaxation rates, T_{1n} and T_{2e} are set as 4 s and 10 μs, respectively, inspired by experimental data.

4. Results and Discussion

4.1 Experimental: Effect of T_{1e} on depolarization

All MAS DNP experiments were carried out at 7 Tesla, at LT of 25 K and relying on a QO-DNP setup powered by a solid-state source yielding a peak μw power of 140 mW, as described in the Methods section. The ^{1}H DNP enhancement $\epsilon_{on/off}$ of each radical solution was determined by calculating the ratio of ^{1}H NMR signal with and without μw irradiation. Figure 2a shows the $\epsilon_{on/off}$ value as the spinning rate is increased from 0 to 5 kHz. The various mono-, bi-, and tri-radicals follow a similar enhancement factor trend with respect to the MAS frequency: there is an initial increase in enhancement from static to ~1 kHz for each radical, with AMUPOL yielding the largest $\epsilon_{on/off}$ of all radicals at 1 kHz spinning rate with an $\epsilon_{on/off}$= 38. As the spinning rate is increased further, there is a significant decline in $\epsilon_{on/off}$ values for all radicals measured. At 3 kHz, the $\epsilon_{on/off}$ of AMUPOL falls below the $\epsilon_{on/off}$ of DOTOPA-ethanol, so that at 5 kHz spinning rate DOTOPA-ethanol yielded the largest enhancement ($\epsilon_{on/off}$ = 17), followed by AMUPOL ($\epsilon_{on/off}$ = 11), TOTAPOL and 4AT, both yielding an $\epsilon_{on/off}$ ~ 5. The $\epsilon_{on/off}$ values are greatest with DOTOPA-ethanol under MAS DNP at 25 K and 7 T. Next, we look into the effect of depolarization and paramagnetic bleaching effects that can lower the baseline NMR signal in the absence of μw irradiation and under MAS.

Figure 2b shows the ^{1}H NMR signal reduction due to depolarization for each radical-solvent system as the spinning rate is increased. Here, the NMR signal was normalized with respect to the ^{1}H NMR signal at 0 kHz spinning rate for each radical, individually. Both bi-radicals, TOTAPOL and AMUPOL, and the tri-radical, DOTOPA-ethanol, yielded greater depolarization with increasing spinning rate, whereas 4AT and the sample without the polarizing agent yield fairly constant ^{1}H NMR signal levels with spinning rate.

This reduction in the ^{1}H NMR signal below the level from thermal polarization with increasing spinning rate is a characteristic of the depolarization effect. The depolarization constant was quantified as the ratio of NMR signal under 5 kHz spinning and static condition, in the absence of μw irradiation, *i.e.*, $\epsilon_{depo} = \langle S_{spin} \rangle / \langle S_{static} \rangle$. Notably, AMUPOL leads to maximum nuclear signal depolarization, with ϵ_{depo}=0.4, leading to an overestimation (or the *depolarization-factor*, $1/\epsilon_{depo}$) by ~2.5 in the DNP enhancement using $\epsilon_{on/off}$.

In order to calculate the absolute sensitivity gain from DNP ($\epsilon_{absolute}$) one must take into account the paramagnetic bleaching effect, where proximity to a free electron spin causes the nuclear T_2 to shorten and broaden the NMR signal beyond detectability.[27,30,41] The paramagnetic bleaching factor (ϵ_{bleach}) is defined as the static (0 kHz) ^{1}H NMR signal intensity without radical in the solvent divided by the ^{1}H NMR signal measured under equivalent conditions with the addition of nitroxide radical. The absolute signal enhancement ($\epsilon_{absolute}$) at 25 K is the $\epsilon_{on/off}$ multiplied by the depolarization, ϵ_{depo} and divided by the paramagnetic bleaching factor, ϵ_{bleach}.

Author Manuscript Author Manuscript Author Manuscript Author Manuscript

$$\epsilon_{absolute} = \epsilon_{on/off} \cdot \epsilon_{depo} \,/\, \epsilon_{bleach} \quad (2)$$

The calculated $\epsilon_{absolute}$ for each radical is shown in Fig. 2c. Here, we see that DOTOPA-ethanol shows marginally larger enhancement compared to the rest of the radicals measured at 1 kHz. But as the spinning rate is increased to 5 kHz, all radicals yielded a rather comparable absolute enhancement factor. Mentink-Vigier *et. al.* performed MAS DNP measurements with a commercial Bruker DNP system at 94 K and 9.4 T, and reported the $\epsilon_{absolute}$ of AMUPOL to be 1.5 times that of TOTAPOL, and contrast it to the $\epsilon_{on/off}$ value for AMUPOL that is 3.3 times that of TOTAPOL.[27] In our QO DNP system at 25 K at 7 T, we observe that accounting for depolarization and paramagnetic bleaching yields comparable $\epsilon_{absolute}$ for AMUPOL and TOTAPOL, though AMUPOL still slightly outperforms TOTAPOL. We hypothesize that this is due to the power limitation of our 140 mW QO DNP system, where the DNP enhancement has not reached its maximum value to more strongly compensate for the depolarization effect. However, the μw power limitation does not prevent us from fully examining the role of T_{1e} on depolarization as no μw is needed for this.

Next, we report on T_{1e} and the depolarization factor measured at comparable temperature and external magnetic field of the DNP measurements. Using a home-built pulsed EPR instrument[35,36] at 7 T we measured the T_{1e} of various DNP polarizing agents in the samples as prepared for DNP, using an echo detected saturation recovery pulse sequence shown in the inset of Fig. 3(a) and at a μw frequency of 193.887 GHz. The resulting saturation recovery decay curve is fit to a bi-exponential,

$$M_t = 1 - a \,.\, exp[-t \,/\, T_{le}] - b \,.\, exp[-t \,/\, T_{SD}] \quad (3)$$

where T_{SD} is the time constant describing the faster spectral diffusion, whose effect becomes visible in the saturation recovery curve as the μw pulses only excite a portion of the nitroxide EPR line, so that spectral diffusion from spins at different EPR frequencies contribute to the signal recovery.[33] The slower time constant is the relevant T_{1e} value. Figure 3(b) shows the measured depolarization factor plotted against the experimentally measured T_{1e} for each frozen radical solution. The plot shows an unmistaken correlation between longer T_{1e} and a greater ^{1}H ϵ_{depo} under MAS at 5 kHz. This demonstrates that one of the key factors leading to significant depolarization observed with AMUPOL under various conditions is its long T_{1e}. In fact, long T_{1e} was among the design principle for AMUPOL, as well as another family of radicals, such as bTUrea and bTbK that should enhance the saturation efficiency with μw power, leading to higher CE, but also to higher depolarization.

Apart from different T_{1e} values, the various radicals studied here also have different spin interaction parameters, such as the relative *g*-tensor orientation, as well as the *e*-*e* dipolar tensor. Thus, to further disentangle the effect of T_{1e} from the other spin dynamics factors, we design an experiment to exclusively alter T_{1e} by adding Gd^{3+} ions at low concentrations of <1 mM where only T_{1e}, but not T_{1n} is measurably shortened, as experimentally

Author Manuscript Author Manuscript Author Manuscript Author Manuscript

demonstrated in previous studies by Walker *et. al.* and Johannesson *et. al.*[48-49] Specifically, $GdCl_3$ was added to the DOTOPA-ethanol solution at two different concentrations of 0.1 mM and 1 mM. We found that the T_{1e} of the DOTOPA-ethanol is reduced from 4 ms to 2 ms with 0.1 mM Gd^{3+}, as well as the *depolarization-factor*, $1/\epsilon_{depo}$ significantly reduced by 32%. Upon addition of the higher $GdCl_3$ concentration of 1 mM to the DOTOPA-ethanol solution, the T_{1e} is reduced from 4 ms to 0.1 ms, and the *depolarization-factor*, $1/\epsilon_{depo}$ reduced by 98 %, and hence essentially no nuclear depolarization was observed. This result clearly demonstrates that given the same CE-inducing *e-e* dipolar interaction network of a given radical system, the extent of depolarization can still be significantly tuned, simply by altering its T_{1e}.

4.2 Experimental: Multi electron-spin effect: Electron Spectral Diffusion Rate on Depolarization

One parameter that has been omitted thus far in our discussion is electron spectral diffusion (eSD), which describes how a network of dipolar coupled electron spins redistributes polarization across the EPR line. The Vega and Goldfarb groups developed a method of measuring and simulating the phenomenological rate constant of eSD (Λ^{eSD}) in static DNP.[42,43] However, the of eSD rate under MAS conditions has not been characterized, neither theoretically nor experimentally. This is due to a large anisotropy of the electron spins, which causes time dependent mixing of electron spin polarization across the EPR line. Experimentally, this measurement requires the capability to perform pulse EPR detection under MAS - no such instrument exists to date. Nevertheless, we can measure Λ^{eSD} (static) through electron-electron double resonance (ELDOR) experiment for different radical systems in static systems, and report on the local and global electron spin network of the different radical system. This will help deconvolute the effect of Λ^{eSD} and T_{1e} on depolarization under MAS conditions.

To begin, we briefly explain the measurement and fit of experimental ELDOR spectra, which has been fit with the ELDOR-model[42] of Vega *et. al.* to extract the phenomenological eSD parameter, Λ^{eSD}. ELDOR is a pump-probe experiment. A saturation pulse (pump) is applied at a frequency of $F_{Saturation}$, which is swept across the EPR line, while the electron detection pulses (probe) are applied using another synthesizer with frequency, F_{detect}. The ELDOR pulse sequence and resulting spectra for F_{detect}=193.52 GHz are shown in Fig. 4a for AMUPOL and 4AT. The ELDOR spectra of all other detection frequencies, and of the other radicals are shown in the SI. The large peak at −390 MHz offset (marked with *1, in Fig. 4a) is where $F_{Saturation} = F_{detect}$. The peaks at −360 MHz and −340 MHz (marked with *3) are representative of the electron hyperfine coupling to ^{14}N and ^{2}H, respectively. The sharp peaks at −90 MHz and −690 MHz offset are due to strong electron hyperfine coupling to ^{1}H (marked with *2). The electron depolarization for positions marked with *2 and *3 are direct observations of the solid-effect transitions ($F_{Saturation}$ or $\omega_{\mu w}=\omega_e \pm \omega_{0n}$) for the various nuclei in the system. The broad peak at the center of the EPR line (*4) is due to spectral diffusion between the spins irradiated at $F_{Saturation}$ and the detected spins at F_{detect}. This effect is most pronounced around the EPR center peak where the largest electron spin population lies. The lack of any observable spectral diffusion for the mono radical implies

Author Manuscript Author Manuscript Author Manuscript Author Manuscript

that the presence of intramolecular *e-e* coupling is critical for spectral diffusion at 20 mM spin concentration.

In the ELDOR model, the simulated nitroxide EPR line that is inhomogeneously broadened due to the anisotropy in the g-tensor is divided into spin-packets of electrons, “bins”, with the same average frequency (ν_j), average polarization (P_e), and equal bin frequency width (Δ_{bin}). Each bin contains a number of electron spins, f_j, given by the normalized EPR lineshape. The polarization of the bins are calculated by solving a set of coupled rate equations for all $P_e(\nu_j)$. The rate constants in these coupled rate equations are dependent on the microwave irradiation frequency, ν_j, and amplitude, $P_e(\nu_j)$, T_{1e}, T_{2e}, and the polarization exchange rate between the bins, $w^{eSD}_{j,j'}$, as defined by the eSD exchange constant (Λ^{eSD}) given in the following equation:

$$w^{eSD}_{j,j'} = \frac{\Lambda^{eSD}}{(\nu_j - \nu_{j'})^2} \quad (4)$$

where ($\nu_j - \nu_{j'}$) is the frequency difference between two bins. The simulated ELDOR profiles are constructed from the experimentally determined values of f_j, T_{1e}, and the total electron spin concentration. To simulate the ELDOR profile, first the nitroxide EPR lineshape was simulated using the EasySpin simulation package for matlab.[44] The simulated EPR line was then divided into frequency bins, and the spectral diffusion rate $w^{eSD}_{j,j'}$ simulated between the different bins using equation (4).

Figure 4b shows a plot mapping the correlation of the Λ^{eSD} value versus the depolarization factor for all radicals measured. Surprisingly, the Λ^{eSD} values for the two bi- and the tri-radical species are the nearly the same at 25 K, while the mono-radical 4AT showed no spectral diffusion. This finding is interesting for reason: it shows that Λ^{eSD} (static) does not have an effect on the differing depolarization factor measured for each frozen radical solution at the same global electron spin concentration of 20 mM and at 25 K, leaving T_{1e} rates as the major modulator of depolarization.

5. Numerical Simulation: Effect of T_{1e} on depolarization

Thus far we have demonstrated experimentally that T_{1e} is a major modulator of nuclear depolarization. In this section, we corroborate our experimental finding with numerical simulation of a model spin system described in Methods. First, the effects of spinning on NMR signal with and without μw irradiation was calculated, as shown in Fig. 5a and b. Figure 5a maps the ^{1}H $\epsilon_{on/off}$ for spinning rate (ν_r) between 250 Hz to 10 kHz, with T_{1e} set to 3 ms and μw power ν_1 (μw) to 0.1 MHz respectively. As expected, the $\epsilon_{on/off}$ initially increases with the spinning frequency and then decreases sharply. Figure 5b shows the calculated nuclear depolarization ϵ_{depo} for the same spinning range for ν_r. As expected, ϵ_{depo} decreases with increasing spinning rate, and consequently the absolute enhancement, $\epsilon_{absolute}$, (Fig. 5c) diminishes more rapidly at higher spinning frequency in comparison to $\epsilon_{on/off}$. For comparison, the $\epsilon_{on/off}$ (gray) and $\epsilon_{absolute}$ (blue) are overlaid in Fig. 4c. In a

Author Manuscript Author Manuscript Author Manuscript Author Manuscript

nutshell, the reason for an initial increase in enhancement from static to spinning followed by a decrease at faster spinning is due to the counteracting effect on $\epsilon_{absolute}$ from CE probability and level crossing rates, both enhanced under MAS.

Next, we showed the dependence of depolarization and enhancement for a fixed spinning frequency (5 kHz) and varying T_{1e} (Fig. 6). The simulated depolarization (ϵ_{depo}) of the ^{1}H NMR signal monotonically decreases with increasing T_{1e} before reaching a plateau value at T_{1e}= ~8ms (Fig. 6a). This is consistent with experimental observation that saw increased depolarization with increased T_{1e} between below 2 to 6 ms (see Fig. 3). On the right-hand y axis, the normalized difference in the two electron spin polarizations, Δe, is plotted with respect to the same x-axis. Remarkably, Δe tracks the same trend as the nuclear depolarization. Lower Δe leads to greater nuclear depolarization, and *vice versa*. This is because the polarization exchange between the CE-fulfilling electron spins and nucleus at the CE *rotor event* is proportional to the polarization difference between the two electrons and nucleus.[23] The μw-driven absolute DNP signal enhancement ($\epsilon_{absolute}$) is also T_{1e} dependent, and in general increases with longer T_{1e} as reflected in Fig. 6b. Interestingly, we observed that there is an optimum value for T_{1e} to reach the maximum DNP enhancement. We also monitored Δe under μw irradiation. Again, Δe tracks the same trend as $\epsilon_{absolute}$. The value for the optimum T_{1e} depends on μw irradiation parameters and spin rate. However, it is evident that a too long T_{1e} is not optimal due to depolarization, and consequently for maximizing the absolute DNP enhancement.

We next dissected the dependence of depolarization on T_{1e} and relative *g*-tensors orientation. The simulations shown so far represent exemplary results for a somewhat randomly chosen *e*-*e*-^{1}*H* system in terms of *g*-tensor orientation and the dipolar coupling tensors for coupled, CE fulfilling, electron spins. It is, however, understood that the relative orientations of the *g*-tensors of the coupled electron spins are important as they determine the resonance conditions leading to both CE and the *e*-*e* polarization exchange, as well as the probability and efficiency of the rotor-synchronous level crossing events. It should be noted that the question we ask is different from that of Mentik-Vigner *et. al.*[27] who studied the effect of powder orientation of a radical (fixed *e*-*e*-^{1}*H* spin system) in the external magnetic field, *i.e.* for different crystal/molecule orientation with respect to external magnetic field in the lab frame, on depolarization. In contrast, the focus of our calculation is to change the radical system itself by varying the relative *g*-tensors orientation and calculate the average depolarization effect for the powder sample.

In Fig. 7, ^{1}H ϵ_{depo} is plotted against T_{1e} for varying β that is associated with the *g*-tensors in the Euler angles set {α,β,γ}, while keeping all the other spin parameters same as in the simulations presented in Figures 5 and 6. Molecule to rotor powder averaging is performed for each of these orientations using a repulsion scheme.[45] We observe that for certain orientations, there is maximum depolarization, especially for the near perpendicular orientation between the two electron spin *g*-tensors (Figure 7, green). Only when the two *g*-tensors are parallel to each other, no depolarization NMR signal is observed (Figure 7, red). This finding was expected, as such orientations will result in the Zeeman energies of the two electron spins to be equal, so that the CE condition that requires their frequency difference to correspond to that of the nuclear Larmor frequency cannot be fulfilled at any rotor position.

Author Manuscript Author Manuscript Author Manuscript Author Manuscript

When averaging over all the selected orientations, we observe smaller nuclear depolarization, with average ^{1}H ϵ_{depo} equalling ~ 0.7 compared to ~ 0.3 for perpendicular orientations for this spin system.

Next, we considered the effect of the *e-e* dipolar coupling tensor on nuclear spin depolarization. In the simulations presented thus far, we have fixed the *e-e* dipolar tensor to the orientation {124°, 94°, 0°} and strength of ~19 MHz (14 Å). To keep it simple, we only change the coupling strength, but keep the dipolar tensor orientations with respect to the *g*-tensors unchanged. The simulated results shows, in Fig. 8a, that there is an intermediate range for the *e-e* dipolar coupling strength that leads to maximum depolarization. Zero *e-e* coupling shows no depolarization, simply because CE Hamiltonian strength is zero. As the *e-e* coupling strength increases the CE Hamiltonian strength also increases, resulting in greater depolarization. The *e-e* coupling strength also determines the magnitude of polarization exchange between the two electrons when they reach degenerate conditions (*i.e.* at *dipolar rotor event*). Therefore, we need to take into account both the *CE rotor event* as well as the *dipolar rotor events*. In a similar context, Mentink-Vigier *et. al.* have statistically predicted that if the dipolar *rotor events* are diabatic (non-adiabatic) in nature (because of small *e-e* coupling) then it leads only to a partial polarization exchange between the two electrons.[27] Such *dipolar rotor event* will have an effect to reduce the polarization difference between two electron, and this can eventually result in larger nuclear depolarization. However, very strong *e-e* dipolar coupling leads to adiabatic crossing that maintains the polarization difference between the electrons spins, resulting in smaller nuclear depolarization at CE *rotor event*. Nonetheless, the depolarization effect cannot be fully nullified by increasing the *e-e* dipolar strength beyond a limit. This is evident in the simulation shown in Fig. 8b that maps ^{1}H ϵ_{depo} as a function of *e-e* dipolar strength, at T_{1e} = 0.3 ms and 3 ms , with all other parameters held the same as in Fig. 8a. Clearly, ^{1}H ϵ_{depo} as a function of *e-e* dipolar coupling strength has the feature of an "*anharmonic potential well*" - for a certain *e-e* coupling value where ϵ_{depo} reaches a minimum (i.e. maximum nuclear depolarization), but at large *e-e* dipolar coupling ϵ_{depo} reaches a plateau whose value is determined by relaxation rates and relative *g*-tensor orientations.

The presence of J-coupling (or exchange coupling) increases the net effect of the *e-e* coupling strength at the rotor crossings, independent of orientations. Strong J-coupling therefore reduces the orientation dependence of the *e-e* dipolar coupling. Furthermore, the relative orientation of the *g*-tensors with respect to the dipole couplings tensor is also critical for CE. This is because the strength of the Hamiltonian at the resonance condition is not the only factor modulating nuclear depolarization, but also the time sequence of various *rotor events*. An in-depth analysis is needed to understand the most favourable spin-interaction orientations for DNP that optimizes both the Hamiltonian and the sequence for the various crossings to maximize the CE, while minimizing nuclear depolarization. This analysis is beyond the scope of the present manuscript.

Finally, we take advantage of the *in-silico* DNP analysis to predict depolarization of a biradical where the two electron spins have different isotropic chemical shifts. Temp-Trityl, a new family of radical, belongs to this category of radicals that have shown to minimize depolarization and maximize DNP enhancement at high magnetic field (^{1}H > 800 MHz).

Author Manuscript Author Manuscript Author Manuscript Author Manuscript

[46,47] Inspired by this, we considered the case of *e*-*e*-^{1}H with one of electrons having *g*-anisotropy of trityl {g_x,g_y,g_z =2.0034, 2.0031, 2.0027} and the other having *g*-anisotropy of nitroxide {g_x,g_y,g_z =2.0094, 2.006, 2.0017}. Figure 9 shows the dependence of ^{1}H ϵ_{depo} on the isotropic chemical shift difference (Δ_{iso}) of these two electrons. Greater nuclear depolarization, or smaller ^{1}H ϵ_{depo} is seen as the absolute Δ_{iso} decreases towards 0. Large Δ_{iso} minimizes the probability of dipolar *rotor event* that tend to reduce the polarization difference between the two CE fulfilling electron spins, and result in smaller nuclear depolarization (larger ^{1}H ϵ_{depo}). When Δ_{iso} is ~ 300 MHz, which corresponds to the average Δ_{iso} between trityl and tempo, the nuclear depolarization is significantly reduced resulting in ^{1}H ϵ_{depo} =0.95. This shows the great potential of narrow-broad combo-radicals as a solution to reduce ^{1}H depolarization, as discussed recently in literature.[47] Also, it is very interesting to note that for certain conditions, ϵ_{depo} can be larger than one. Theoretically both enhancement as well as depolarization of nuclear spin is possible owing to the same CE under MAS, depending on the electron polarization gradient.

Taken together, these simulations demonstrated that T_{1e}, the spin rate, the two electrons spin *g*-tensor orientation, and the *e*-*e* dipolar coupling all influence nuclear depolarization due to CE under MAS. Using these results, we analyzed the experimental results shown in Figures 2 and 3. It was observed that AMUPOL leads to maximum depolarization. Relatively long T_{1e} of AMUPOL, owing to its rigidity, is likely the primary cause of the large depolarization seen with AMUPOL. In addition, close to perpendicular orientation of the nitroxides in AMUPOL also contributes to its depolarization. TOTAPOL has similar dipolar coupling strengths as AMUPOL, while it populates a wide range of relative *g*-tensor orientations. We can rationalize the smaller depolarization effect seen with TOTAPOL with the shorter T_{1e} of TOTAPOL compared to AMUPOL. In case of 4AT, which is a mono-radical, the averaging over both *g*-tensors and dipolar couplings between the two random orientations satisfying CE may reduce the nuclear depolarization, but this is difficult to evaluate without considering a greater *e*-*e* ensemble representing 4AT in solution. It should be noted that the reduction in nuclear depolarization owing to non-optimally oriented *g*-tensors and small dipolar coupling also attenuates the CE enhancement.

What is clear is that the experimental results with a diverse set of commonly used radicals for DNP of 4AT, TOTAPOL, AMUPOL and DOTOPA-ethanol, and with the addition of $GdCl_3$, showed a clear correlation between T_{1e} and ϵ_{depo}. This means that the differences in the other factors, such as *e*-*e* dipolar coupling strengths and relative *g*-tensor orientation, are less dominant factors in these systems. This is further corroborated by our finding that the empirical spectral diffusion parameter, Λ^{eSD}, under static condition is indistinguishable between these different radical systems studied here. While the physical interpretation of Λ^{eSD} is subject of ongoing studies by Vega and coworkers,[42,43] these results show that the average *e*-*e* dipolar coupling network is comparable between the different bi- and tri-radical systems, ensured by keeping the total electron spin concentration constant (here at 20 mM). For achieving high absolute DNP enhancements, focusing on modulating T_{1e} is hence a promising approach to optimize $\epsilon_{absolute}$, once radical systems with promising CE DNP performance have been identified. We demonstrated such an example: the effect of depolarization in DOTOPA-ethanol can be nullified simply by reducing it's T_{1e} upon doping with adequate concentrations of $GdCl_3$ dopants.

Author Manuscript Author Manuscript Author Manuscript Author Manuscript

6. Conclusion and Outlook

In this study we carried out MAS DNP experiments at 25 K and 7 Tesla, and showed that nuclear depolarization can cause an inflated $\epsilon_{on/off}$ by up to 60 % with commonly used bi- and tri- nitroxide radicals at 20 mM global electron spin concentration. The mono-radical at 20 mM spin concentration showed no significant depolarization. The nuclear depolarization effect is owing to an equalization of the electron spin polarization across the EPR line facilitated by MAS, where the extent of this depolarization is strongly influenced by the T_{1e} of the nitroxide radicals. Consequently, the deliberate shortening of T_{1e} by the addition of a paramagnetic relaxing agent such at Gd^{3+} to the nitroxide spin system reduced the nuclear depolarization effect. The experimental studies were accompanied with fully quantum mechanical numerical simulations of depolarization effects, enabled by the SPIN-EVOLUTION package. These simulations showed that T_{1e} is indeed a major modulator of nuclear depolarization, but that other factors, such as the two electron spin relative *g*-tensor orientation and the *e-e* dipolar coupling, also influence nuclear depolarization under MAS, consistent with findings in the literature.[26,27] Intriguingly, the experimental results showed that setting the global electron spin concentration to 20 mM for commonly used nitroxide radicals was sufficient to keep all factors sufficiently comparable, so that T_{1e} was the dominant modulator. This was corroborated with two-frequency ELDOR experiments carried out under static conditions that extracted *phenomenological* spectral diffusion rate constants that were found to be within error for the bi-, and tri- nitroxide radical systems under the here used experimental conditions. The extent to which spectral diffusion plays a role in equalizing the electron spin polarization in the CE process and its effect on nuclear depolarization have not been discussed in the literature, and should be subject of future studies. When entirely different radical systems are considered for MAS DNP, *e.g.* narrow-broad mixed radicals, radicals with different *g*-anisotropy and tensor orientation, or strongly coupled radicals, the predominance of T_{1e} in modulating nuclear depolarization may not hold. In fact, if a radical could be designed whose CE fulfilling electron spin pairs do not exchange electron spin polarization (non-overlapping), depolarization effects should be minimal under MAS.

Supplementary Material

Refer to Web version on PubMed Central for supplementary material.

Acknowledgements

This work was supported by the National Science Foundation (NSF) (CHE #1505038 to S.H.), the National Institute of Health (NIH) (NIBIB #R21EB022731 and #R21GM103477 to S.H.) and the Binational Science Foundation (Grant #2014149 to S.H.). R. Tycko is acknowledged for providing us with DOTOPA-ethanol. We thank the Vega group for providing us with the model and simulation programs for DNP-ELDOR data. We also thank Revolution NMR, specifically David Lewis and Ed Twehous for their continued support and help with the DNP probe. The content is solely the responsibility of the authors and does not necessarily represent the official views of the National Institutes of Health.

Notes and references

1. Bayro MJ, Debelouchina GT, Eddy MT, Birkett NR, MacPhee CE, Rosay M, Maas WE, Dobson CM and Griffin RG, J. Am. Chem. Soc, 2011, 133, 13967–74. [PubMed: 21774549]

Author Manuscript Author Manuscript Author Manuscript Author Manuscript

2. Hall DA, Maus DC, Gerfen GJ, Inati SJ, Becerra LR, Dahlquist FW and Griffin RG, Science, 1997, 276, 930. [PubMed: 9139651]

3. Barnes AB, De Paëpe G, van der Wel PCA, Hu K-N, Joo C-G, Bajaj VS, Mak-Jurkauskas ML, Sirigiri JR, Herzfeld J, Temkin RJ, and Griffin RG, Appl. Magn. Reson, 2008, 34, 237. [PubMed: 19194532]

4. Pourpoint F, Thankamony ASL, Volkringer C, Loiseau T, Trébosc J, Aussenac F, Carnevale D, Bodenhausen G, Vezin H, Lafon O and Amoureux J-P, Chem. Commun, 2014, 50, 933.

5. Lee D, Takahashi H, Thankamony ASL, Dacquin J-P, Bardet M, Lafon O and De Paëpe G, J. Am. Chem. Soc, 2012, 134, 18491. [PubMed: 23095121]

6. Rossini AJ, Zagdoun A, Lelli M, Lesage A, Copéret C and Emsley L, Acc. Chem. Res, 2013, 46, 1942. [PubMed: 23517009]

7. Perras FA, Kobayashi T and Pruski M, J. Am. Chem. Soc, 2015, 137, 8336. [PubMed: 26098846]

8. Rossini AJ, Zagdoun A, Lelli M, Gajan D, Rascon F, Rosay M, Maas WE, Coperet C, Lesage A and Emsley L, Chem. Sci, 2012, 3, 108–115.

9. Veinberg SL, Johnston KE, Jaroszewicz MJ, Kispal BM, Mireault CR, Kobayashi T, Pruski M and Schurko RW, Phys. Chem. Chem. Phys, 2016, 18, 17713–17730. [PubMed: 27314503]

10. Song C, Hu KN, Joo CG, Swager TM, and Griffin RG, J. Am. Chem. Soc, 2006, 128, 11385. [PubMed: 16939261]

11. Dane EL, Corzilius B, Rizzato E, Stocker P, Maly T, Smith AA, Griffin RG, Ouari O, Tordo P and Swager TM, J. Org. Chem, 2012, 77, 1789. [PubMed: 22304384]

12. Matsuki Y, Maly T, Ouari O, Karoui H, Le Moigne F, Rizzato E, Lyubenova S, Herzfeld J, Prisner T, Tordo P and Griffin RG, Angew. Chem., Int. Ed, 2009, 48, 4996.

13. Hu KN, Song C, Yu H, Swager T and Griffin RG, J. Chem. Phys, 2008, 128, 052302. [PubMed: 18266419]

14. Lelli M, Rossini AJ, Casano G, Ouari O, Tordo P, Lesagea A and Emsley L, Chem. Commun. (Camb), 2014, 50, 10198. [PubMed: 24871229]

15. Zagdoun A, Casano G, Ouari O, Schwarzwälder M, Rossini AJ, Aussenac F, Yulikov M, Jeschke G, Copéret C, Lesage A, Tordo P and Emsley L, J. Am. Chem. Soc, 2013, 135, 12790. [PubMed: 23961876]

16. Kubicki DJ, Casano G, Schwarzwälder M, Abel S, Sauvée C, Ganesan K, Yulikov M, Rossini AJ, Jeschke G, Copéret C, Lesage A, Tordo P, Ouari O and Emsley L, Chem. Sci, 2016, 7, 550. [PubMed: 29896347]

17. Can TV, Caporini MA, Mentink-Vigier F, Corzilius B, Walish JJ, Rosay M, Maas WE, Baldus M, Vega S, Swager TM and Griffin RG, J. Chem. Phys, 2014, 141, 064202. [PubMed: 25134564]

18. Sauvee C, Rosay M, Casano G, Aussenac F, Weber RT, Ouari O and Tordo P, Angew. Chem., Int. Ed, 2013, 52, 10858.

19. Yau W-M, Thurber KR and Tycko R, J. Magn. Res, 2014, 244, 98.

20. Michaelis VK, Smith AA, Corzilius B, Haze O, Swager TM and Griffin RG, J. Am. Chem. Soc, 2013, 135, 2935. [PubMed: 23373472]

21. Hu KN, Bajaj VS, Rosay M and Griffin RG, J. Chem. Phys, 2007, 126, 044512. [PubMed: 17286492]

22. Veshtort M, and Griffin RG, J. Magn. Reson, 2006, 178, 248. [PubMed: 16338152]

23. Mentink-Vigier F, Akbey U, Oschkinat H, Vega S and Feintuch A, J. Magn. Reson, 2015, 258, 102. [PubMed: 26232770]

24. Mentink-Vigier F, Akbey U, Hovav Y, Vega S, Oschkinat H and Feintuch A, J. Magn. Reson, 2012, 224, 13. [PubMed: 23000976]

25. Thurber KR and Tycko R, J. Chem. Phys, 2012, 137, 084508. [PubMed: 22938251]

26. Thurber KR and Tycko R, J. Chem. Phys, 2014, 140, 184201. [PubMed: 24832263]

27. Mentink-Vigier F, Vega S and Paëpe GD, Phys. Chem. Chem. Phys, 2015, 17, 21824–21836. [PubMed: 26235749]

28. Jefferies CD, Phys. Rev, 1957, 106, 164–165.

29. Zener C, Proc. R. Soc. A, 1932, 137, 696.

Author Manuscript Author Manuscript Author Manuscript Author Manuscript

30. Corzilius B, Andreas LB, Smith A. a., Ni QZ and Griffin RG, J. Magn. Reson, 2014, 240, 113. [PubMed: 24394190]
31. Mentink-Vigier F, Vega S. and Paëpe GD, Phys. Chem. Chem. Phys, 2017, 19, 3506. [PubMed: 28093594]
32. Thurber KR, Potapov A, Yau W-M and Tycko R, J. Magn. Reson, 2013, 226, 100. [PubMed: 23238592]
33. Thurber KR and Tycko R, J. Magn. Reson, 2016, 264, 99. [PubMed: 26920835]
34. Thurber KR and Tycko R, J. Magn. Reson, 2008, 195, 179–196. [PubMed: 18922715]
35. Siaw TA, Leavesley A, Lund A, Kaminker I and Han S, J. Magn. Reson, 2016, 264, 131. [PubMed: 26920839]
36. Kaminker I, Barnes R and Han S, J. Magn. Reson, 2017, 279, 81. [PubMed: 28482216]
37. Leavesley A, Kaminker I and Han S, John Wiley & Sons, 2018, ISBN 9781119441649.
38. Equbal A, Li Y, Leavesley A, Huang S, Rajca S, Rajca A and Han S, J. Phyc. Chem. Lett, 2018, 9, 2175.
39. Hogben M, Krzystyniak M, Charnock GTP, Hore PJ and Kuprov I, J. Magn. Reson, 2011, 208, 179. [PubMed: 21169043]
40. Bak M, Rasmussen JT and Nielsen NC, J. Magn. Reson, 2000, 147, 296. [PubMed: 11097821]
41. Takahashi H, Fernández-De-Alba C, Lee D, Maurel V, Gambarelli S, Bardet M, Hediger S, Barra AL and De Paëpe G, J. Magn. Reson, 2014, 239, 91. [PubMed: 24480716]
42. Hovav Y, Kaminker I, Shimon D, Feintuch A, Goldfarb D and Vega S, Phys. Chem. Chem. Phys, 2015, 17, 226. [PubMed: 25384575]
43. Hovav Y, Shimon D, Kaminker I, Feintuch A, Goldfarb D and Vega S, Phys. Chem. Chem. Phys, 2015, 17, 6053. [PubMed: 25640165]
44. Stoll S and Schweiger A, J. Magn. Reson, 2006, 178, 42. [PubMed: 16188474]
45. Bak M and Nielsen NC, J. Magn. Reson, 1997, 125, 132. [PubMed: 9245368]
46. Mathies G, Caporini MA, Michaelis VK, Liu Y, Hu KN, Mance D, Zweier JL, Rosay M, Baldus M and Griffin RG, Angew. Chem., Int. Ed, 2015, 54, 11770.
47. Mentink-Vigier F, Mathies G, Liu Y, Barra A, Caporini MA, Lee D, Hediger S, Griffin RG and Paëpe GD, Chem. Sci, 2017, 8, 8150. [PubMed: 29619170]
48. Walker S, Edwards DT, Siaw TA, Armstrong BD and Han S, Phys. Chem. Chem. Phys, 2013, 15, 15106. [PubMed: 23925724]
49. Johannessom H, Macholl S and Larsen JHA, J. Magn. Reson, 2009, 197, 167. [PubMed: 19162518]

Author Manuscript Author Manuscript Author Manuscript Author Manuscript

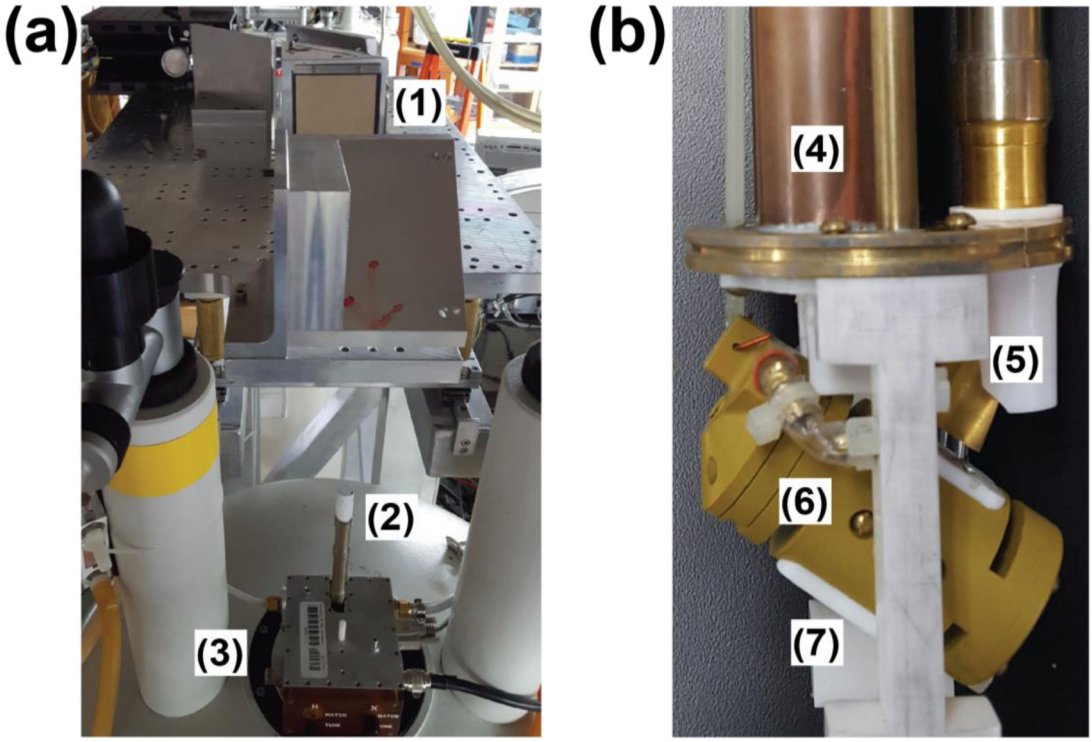

Figure 1.

(a) Quasi-optical Bridge with (1) isolator and two focusing parabolic mirrors, (2) microwave waveguide extending from top of (3) 4 mm Revolution NMR LLC. probe. (b) Bottom of probe head, (4) radio frequency transmission line, (5) Thomas Keating Ltd. Corrugated waveguide with miter bend, (6) stator, and (7) cooling helium gas inlet.

Author Manuscript Author Manuscript Author Manuscript Author Manuscript

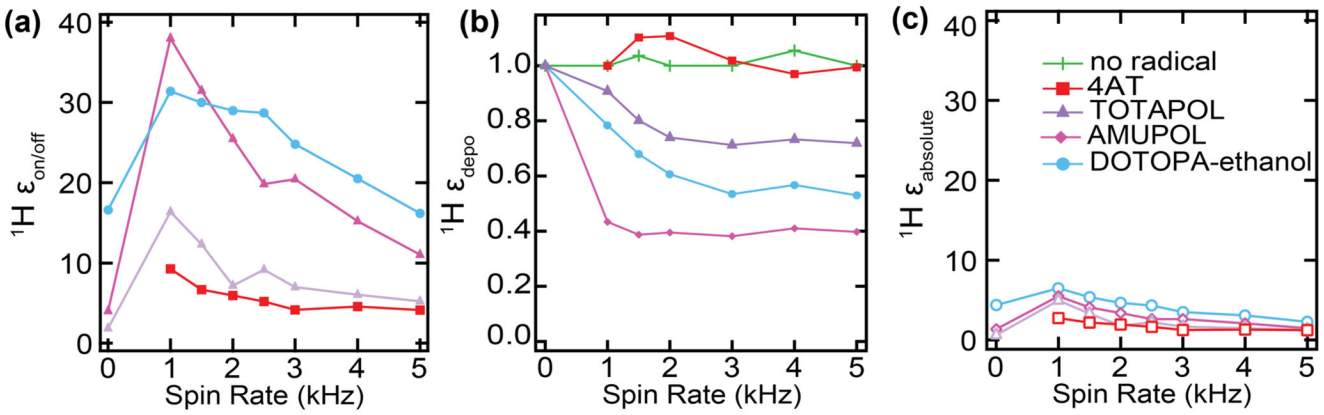

Figure 2.

(a) Enhancement ($\epsilon_{on/off}$) vs. spin rate at ~7 T, the enhancement was calculated from μw_on / μw_off signal of 4AT (red), TOTAPOL (purple), AMUPOL (pink), and DOTOPA-ethanol (blue). (b) The NMR signal (ϵ_{depo}) vs. spin rate without microwave irradiations, normalized to the NMR signal at 0 kHz. (c) The absolute ^{1}H NMR signal enhancement ($\epsilon_{absolute}$) vs. spin rate for each radical frozen solution after correcting for paramagnetic bleaching and depolarization effect. Temperature was set to 25 K. ^{1}H signal was directly detected using 10 s build up time.

Author Manuscript Author Manuscript Author Manuscript Author Manuscript

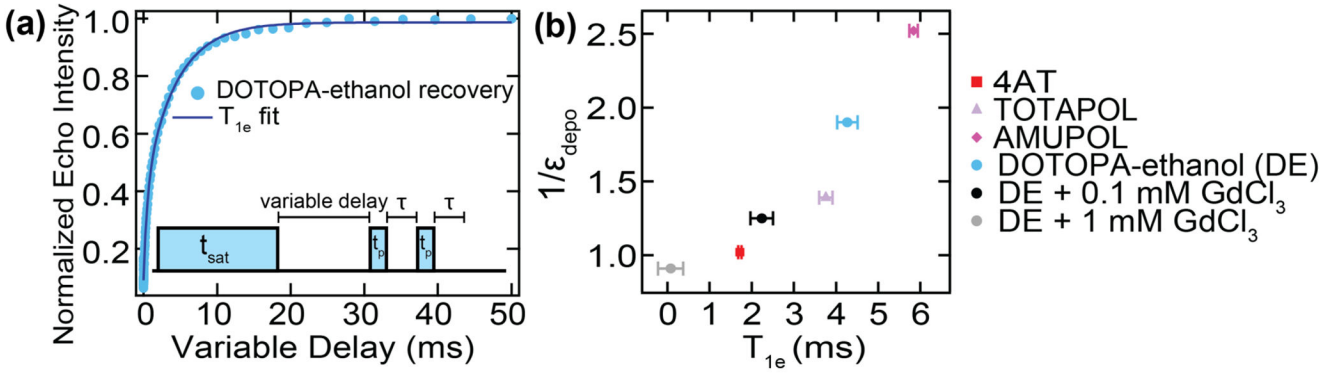

Figure 3.

(a) Pulse schematic of saturation recovery experiment for T_{1e} measurement. T_{1e} fit of DOTOPA-ethanol saturation recovery curve. (b) Depolarization factor, $1/\epsilon_{depo}$, measured (using direct ^{1}H detection at 5 kHz spinning) vs. T_{1e} of all radicals measured at 25 K.

Author Manuscript Author Manuscript Author Manuscript Author Manuscript

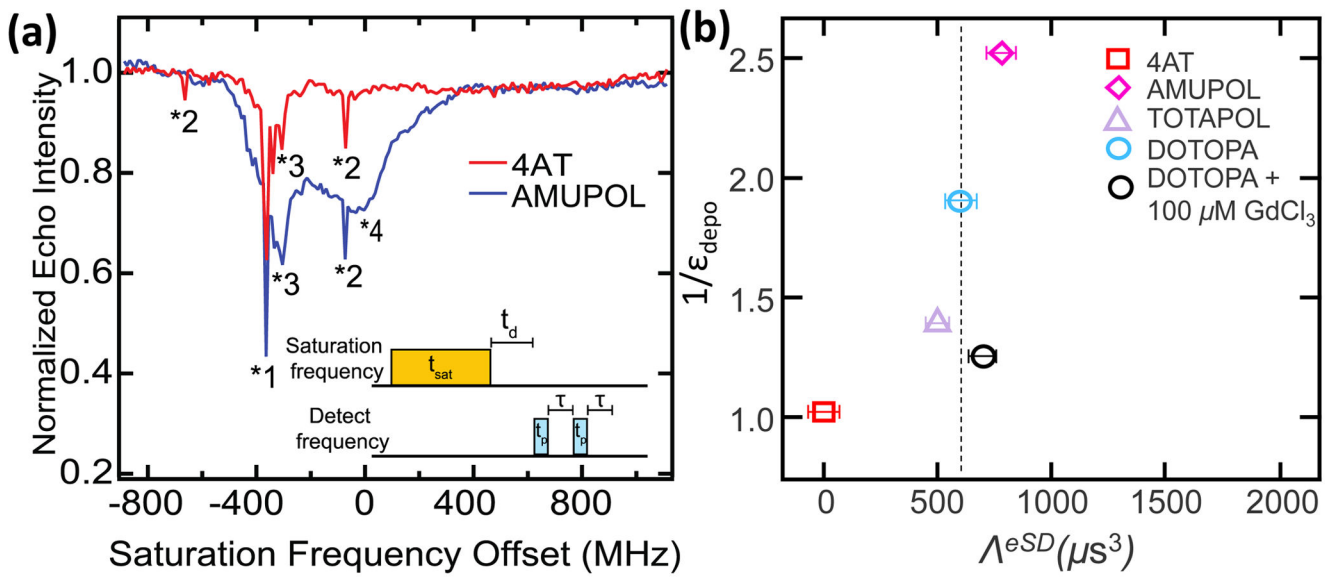

Figure 4.

(a) ELDOR spectrum of 4-amino TEMPO (4AT) and AMUPOL at a detection frequency of 193.52 GHz (or −390 MHz, offset), and at 25 K. Peak labels are as follows: (*1) where the detection frequency equals the saturation frequency, (*2) Hyperfine coupling to the ^{1}H spin in system, (*i.e.* ^{1}H solid effect), (*3) hyperfine coupling to ^{2}H and ^{14}N, and (*4) broad peak at center of the EPR line due to spectral diffusion between irradiated and detected electron spins. (b) Correlation of Depolarization factor, $1/\epsilon_{depo}$, measured (at 5 KHz) vs. Λ^{eSD} of all radicals measured at static condition in an ELDOR experiment depicted in figure 4 (a).

Author Manuscript Author Manuscript Author Manuscript Author Manuscript

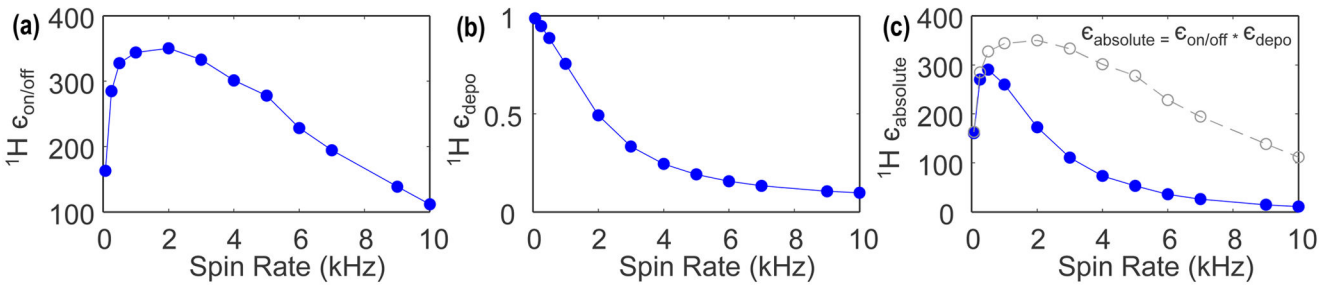

Figure 5.

Numerically simulated ^{1}H enhancement and depolarization for *e-e-^{1}H* spin system at ~7 T (^{1}H frequency = 294.026 MHz) as a function of spin rate for T_{1e} fixed to 3 ms. $\epsilon_{on/off}$, ϵ_{depo}, and $\epsilon_{absolute}$ are plotted in blue in (a), (b), and (c), respectively. In (c), $\epsilon_{on/off}$ is overlaid in gray. All the spin parameters are given in method section. μw power was set to 0.1 MHz.

Author Manuscript Author Manuscript Author Manuscript Author Manuscript

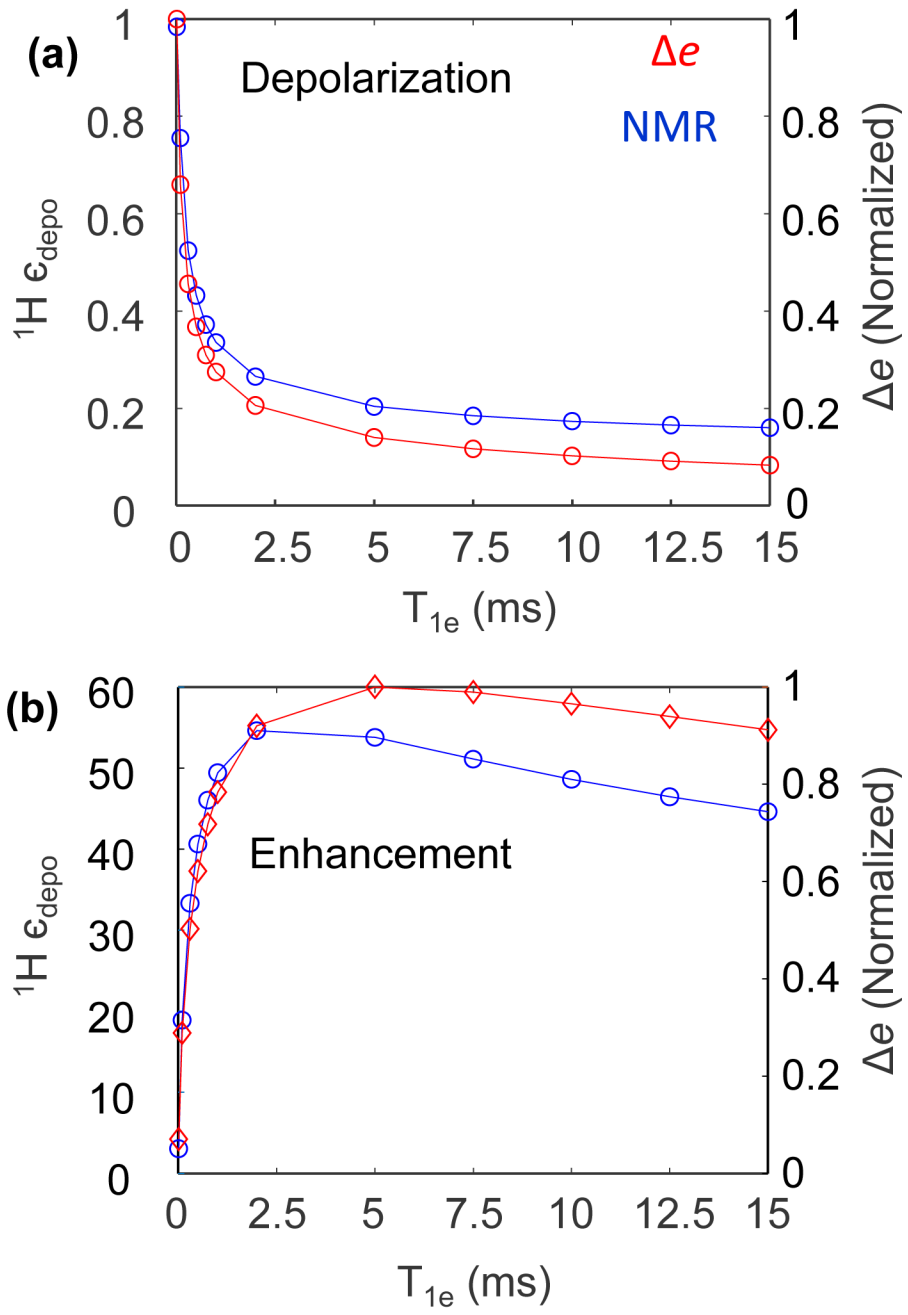

Figure 6.

Numerically simulated (a) depolarization and (b) enhancement for *e-e-*^{1}*H* spin system at 7 T as a function of T_{1e} at 5 kHz spinning (Blue). 0.1 MHz MW power was used for (b). Corresponding electron polarizations difference is also plotted in red. All the spin parameters are the same as in Fig. 5.

Author Manuscript Author Manuscript Author Manuscript Author Manuscript

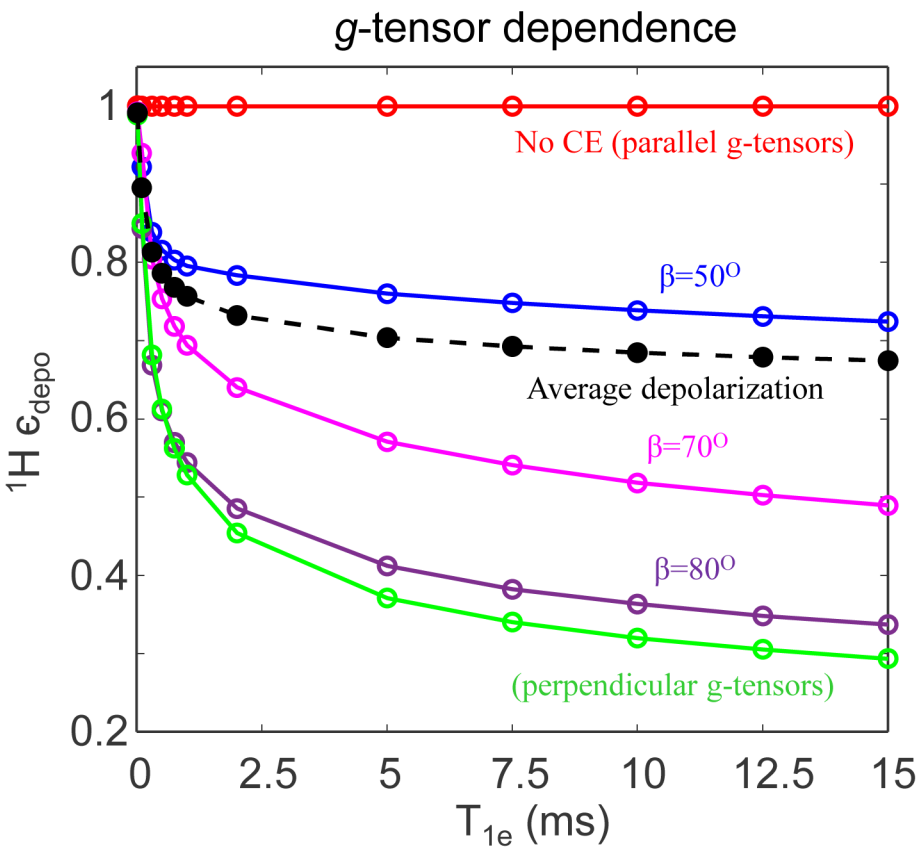

Figure 7:

Numerically simulated depolarization for *e-e-*^{1}*H* spin system at 7 T as a function of T_{1e} at 5 kHz spinning for different relative *g*-tensor orientations. All the spin parameters are the same as earlier. Only the orientation of electron-2 in the spin system is changed by varying β in the euler angle set {0,β,0}.

Author Manuscript Author Manuscript Author Manuscript Author Manuscript

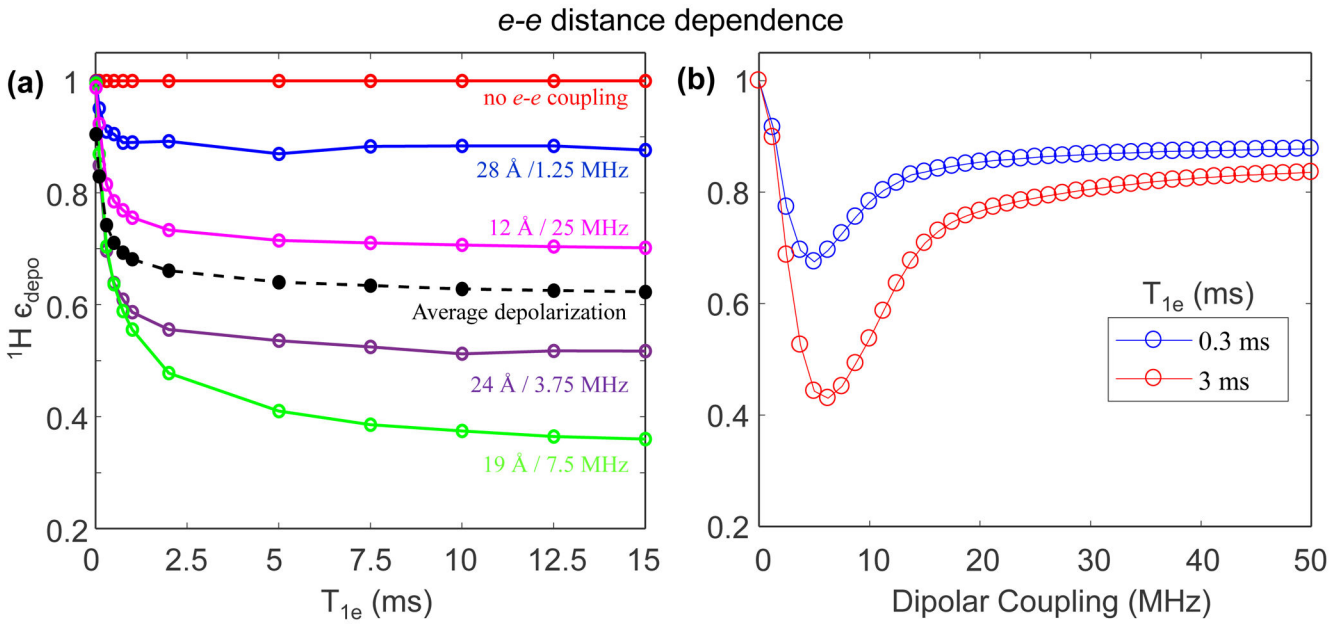

Figure 8.

(a) Numerically simulated depolarization for *e-e-*^{1}H spin system at 7 T as a function of T_{1e} at 5 kHz spinning for different *e-e* distance/dipolar coupling in the spin system described earlier. All the spin parameters are the same as described earlier. (b) Numerically simulated depolarization as a function of dipolar coupling for T_{1e} set to 0.3 ms (blue) and 3 ms (red) at 5 kHz spinning using the same spin system.

Author Manuscript Author Manuscript Author Manuscript Author Manuscript

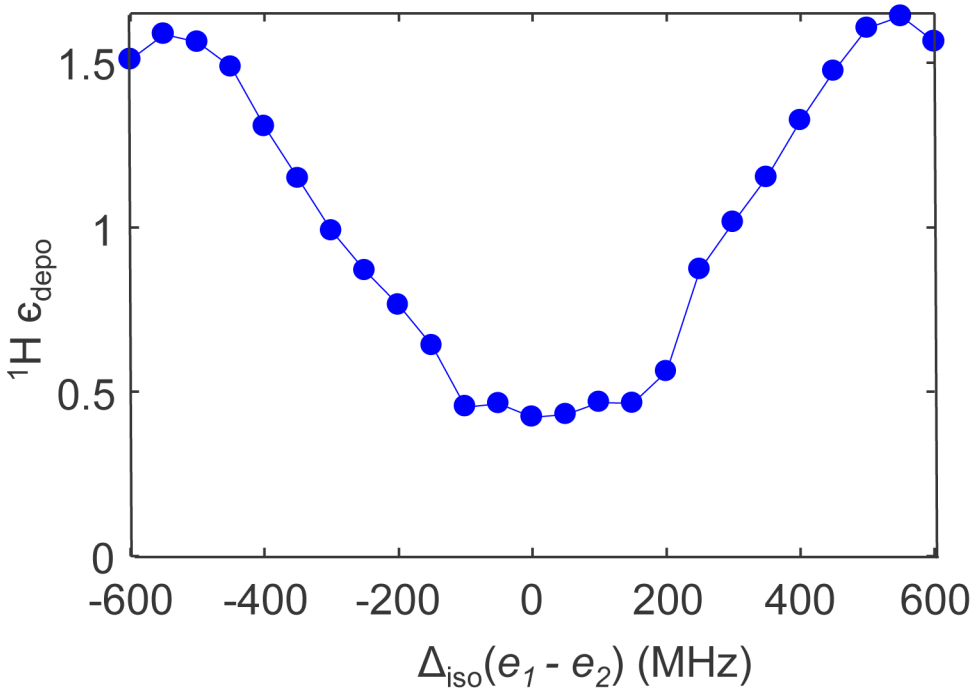

Figure 9.

Numerically simulated depolarization for *e-e-*^{1}*H* spin system at 7 T as a function of difference in the isotropic chemical shift of a narrow radical (like trityl) and broad radical (like 4AT) at 5 kHz spinning using the coupling interaction tensors same as in Fig. 5.